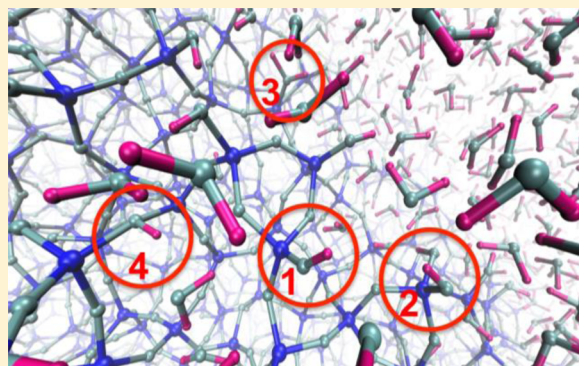


# Proton Dynamics at the Water–Silica Interface via Dissociative Molecular Dynamics

Glenn K. Lockwood and Stephen H. Garofalini\*

Interfacial Molecular Science Laboratory, Department of Materials Science and Engineering, Rutgers University, 607 Taylor Road, Piscataway, New Jersey 08855, United States

**ABSTRACT:** A robust and accurate dissociative potential that reproduces the structural and dynamic properties of bulk and nanoconfined water, and proton transport similar to ab initio calculations in bulk water, is used for reactive molecular dynamics simulations of the proton dynamics at the silica/water interface. The simulations are used to evaluate the lifetimes of protonated sites at the interfaces of water with planar amorphous silica surfaces and cylindrical pores in amorphous silica with different densities of water confined in the pores. In addition to lifetimes, the donor/acceptor sites are evaluated and discussed in terms of local atomistic structure. The results of the lifetimes of the protonated sites, including  $\text{H}_3\text{O}^+$ ,  $\text{SiOH}$ ,  $\text{SiOH}_2^+$ , and  $\text{Si}-(\text{OH}^+)-\text{Si}$  sites, are considered. The lifetime of the hydronium ion,  $\text{H}_3\text{O}^+$ , is considerably shorter near the interface than in bulk water, as are the lifetimes of the other protonated sites. The results indicate the beneficial effect of the amorphous silica surface in enhancing proton transport in wet silica as seen in electrochemical studies and provide the specific molecular mechanisms.



## I. INTRODUCTION

The behavior of excess protons in aqueous environments governs a tremendous range of scientifically and technologically important phenomena and has been the focus of considerable research for decades. Water shows abnormally high proton conductivity as a result of the Grotthuss mechanism, whereby the excess charge moves via proton transfers between neighboring water molecules rather than the diffusion of a single  $\text{H}_3\text{O}^+$  molecule. This structural diffusion mechanism has been studied extensively using quantum mechanical (QM) calculations,<sup>1</sup> multistate empirical valence bond (MS-EVB) molecular dynamics (MD) simulation,<sup>2–4</sup> ultrafast spectroscopy,<sup>5</sup> molecular dynamics (MD) simulations,<sup>6</sup> combined QM/MM,<sup>7</sup> and nuclear magnetic resonance.<sup>8</sup> As a result of these efforts, a consistent picture of how this proton transfer process occurs has emerged.

While the protons of a hydronium ion readily “rattle” between molecules in the ion’s first hydration shell,<sup>2,6,9,10</sup> the transfer only takes place when a hydrogen bond in the second solvation shell breaks and allows the hydronium ion to approach one of its first solvation neighbors to form a Zundel complex. In addition, ultrafast spectroscopy and molecular dynamics have revealed that the effect of excess protons in solution extends to at least the second solvation shell,<sup>11,12</sup> and these observations underline the importance of the local hydrogen bonding environment in understanding the dynamic behavior of solvated protons.

The processes governing proton transport are much less well-defined near interfaces, where the hydrogen bonding network is disrupted<sup>13–16</sup> and the potential energy landscape is

dramatically different from bulk water.<sup>17</sup> In particular, understanding proton transport at the water–silica interface has posed considerable challenges due in part to the amorphous nature of vitreous silica and the extreme degree of atomistic heterogeneity at its surfaces. The importance of proton transport near the water–silica interface has a wide breadth of scientific relevance though. For example, many natural processes such as acid-catalyzed mineral dissolution are governed by the mobility and chemical behavior of protons as they interact with various surface sites.<sup>18–21</sup> Additionally, proton mobility on silica surfaces has significant technological relevance; mesoporous silica exhibits anomalously high proton conductivity.<sup>22,23</sup>

Understanding the behavior of excess protons near the silica surface is of fundamental importance in engineering materials to capitalize upon or minimize certain properties of these applications. Significant effort has been made to characterize the water–silica interface both experimentally and computationally, and the traditionally held view that the hydrated silica surface is composed of silanol ( $\text{SiOH}$ ) groups has been greatly expanded upon in the last two decades.  $\text{SiOH}$  can be classified into one of two groups based on the structure surrounding the Si:  $\text{Q}^3$  silanol, where the Si has three bridging oxygen neighbors, or  $\text{Q}^2$  “geminal” silanol, where the Si has only two bridging oxygen neighbors. These sites show distinct NMR chemical shifts<sup>24–27</sup> and have been postulated to be relevant to

Received: July 29, 2014

Revised: November 24, 2014

Published: December 10, 2014



the bimodal  $pK_a$  observed of the silica surface.<sup>28,29</sup> However, SiOH species can also be classified according to whether or not they are hydrogen bonded, and this distinction has also been put forward as a cause of this bimodal behavior.<sup>30–32</sup>

Most recently, simulation and experiment have provided evidence of two additional acidic sites on silica surfaces that have been studied far less.  $\text{SiOH}_2^+$  has been observed in experiment<sup>33,34</sup> and later simulations,<sup>35,36</sup> and the protonated bridge,  $\text{Si}-(\text{OH}^+)-\text{Si}$ , has been observed in both QM and MD simulations of silica surfaces.<sup>20,36,37</sup> However, these two sites remain largely uncharacterized despite their potential importance in many fundamental processes that give rise to the transport behavior of protons along the silica surface.

To this end, molecular dynamics simulations that utilize a dissociative model<sup>38</sup> of water have been applied here to study the behavior of the protonated sites that exist at the water–silica interface. This model reproduces an extremely wide range of behavior exhibited by water and water–silica interfaces including the adsorption and reaction of water on silica surface sites<sup>38</sup> and the formation of protons near the interface,<sup>35,36</sup> the high thermal expansion of nanoconfined water,<sup>17,39</sup> the restricted transport of water near an interface,<sup>40</sup> the mechanism for proton transport in bulk water,<sup>6</sup> and the activation barrier for dissolution of amorphous silica.<sup>41</sup> In addition, it is computationally efficient and can simulate the extended amorphous silica surfaces required to fully sample the atomic-scale heterogeneity of these materials and capture a wide range of variations in local environment. This combination of reactivity and computational simplicity enables the simulation of proton dynamics at the water–silica interface without having to specify the surface chemistry a priori, providing a comprehensive yet unbiased view of the interfacial properties.

## II. COMPUTATIONAL METHOD

**A. Interatomic Potential.** Molecular dynamics simulations were carried out using a model interatomic potential composed of two- and three-body terms that allow all atoms to interact with all other atoms within a radial cutoff. As a result, no distinction between bonded and nonbonded forces is made, and protons are free to transfer between water molecules and surface sites. This dissociative water potential was parameterized to reproduce the density–temperature curve and structure of bulk water, but also matches other bulk water properties such as the heat of vaporization (within 0.05 kcal/mol of experiment), diffusion coefficient ( $0.24 \text{ \AA}^2/\text{ps}$  vs  $0.23 \text{ \AA}^2/\text{ps}$  experiment at 298 K), and frequency spectrum.<sup>38</sup> It shows proton transport in bulk water with the mechanism and activation barrier consistent with ab initio calculations.<sup>6</sup> Proton transport using this potential shows the expected Eigen and Zundel complexes, with a decrease in the barrier to proton transport with a decrease in O–O spacing in the Zundel complex. Figure 1 shows an  $\text{H}_3\text{O}^+$  ion in the Eigen complex in bulk water simulated with this potential in which the O–O spacing indicated fluctuates around 2.75 Å. Later, this first shell water gets close to the  $\text{H}_3\text{O}^+$  ion as other first shell waters move away, forming a Zundel complex. At this closer spacing (less than 2.5 Å), the proton transfers. This is consistent with the lowering of the free energy barrier to proton transport with decreasing O–O spacing observed in our earlier potential of mean force simulations<sup>6</sup> and others' ab initio calculations.<sup>42</sup> At 2.4 Å, we obtain a barrier of 0.8 kcal/mol<sup>6</sup> while the ab initio calculations by Marx et al. obtain a barrier of 0.6 kcal/mol with a classical proton.<sup>42</sup> The diffusion coefficient for proton

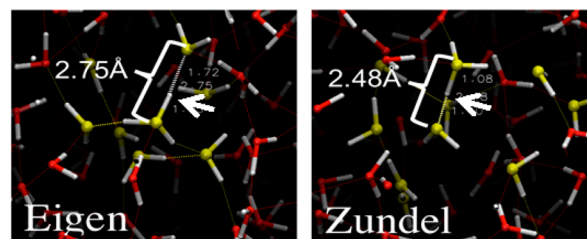


**Figure 1.** Proton transfer in a bulk water simulation showing formation of Eigen and Zundel complexes and the transfer of the proton when the O–O spacing between the  $\text{H}_3\text{O}^+$  ion and a first shell water drops below 2.5 Å. Arrow at transferring proton. The other yellow O eventually become  $\text{H}_3\text{O}^+$  ions during the course of the simulation.

transport using this potential has been calculated by Hofer et al.<sup>7</sup> and is similar to the MS-EVB3 model ( $0.38 \text{ \AA}^2/\text{ps}$  our potential vs  $0.36 \text{ \AA}^2/\text{ps}$  MS-EVB3), each lower than experiment.

The addition of silica was evaluated using the water molecule/silicic acid interaction.<sup>35</sup> The potential is highly transferrable in that it reproduces the behavior of silica and water–silica interfaces in different contexts. In addition to showing hydroxylation of the silica surface, the simulations show hydronium ion formation near the water/silica interface,<sup>35</sup> similar to ab initio MD simulations.<sup>43</sup> One example is shown in Figure 2. The top images are snapshots from an MD simulation using this potential of water vapor interacting with the silica surface; the lower images are from an ab initio MD simulation by Ma et al.<sup>43</sup> Arrows point to the adsorption of the water molecule (2a) and subsequent transfer of the proton via formation of  $\text{H}_3\text{O}^+$  ions (2b,c), to a nonbridging oxygen (2d) in both simulations.

The potential also reproduces the excessively high thermal expansion coefficient observed experimentally for nanoconfined water in mesoporous silica as a function of pore size.<sup>17,39</sup> MD simulations of the diffusion coefficient of water (using the O) in nanoconfinement in 3 nm planar films and a 3 nm diameter cylinder (systems 1 and 3, Table 1) in amorphous silica showed changes in comparison to bulk water, as shown in Figure 3. Diffusion of O in water within 0.6 nm of the interface in the planar system is  $\sim 0.29 \times 10^{-5} \text{ cm}^2/\text{s}$ , considerably lower than the bulk water value. The presence of the interface with amorphous silica clearly slowed the overall diffusion constant in comparison to water away from the interfaces (All  $\text{H}_2\text{O}$  vs Interior  $\text{H}_2\text{O}$ ). In addition, the dissolution of amorphous silica with an activation barrier consistent with experimental data<sup>41</sup> was observed using this potential.

The two-body component is composed of Coulomb interactions between point- and diffuse-charges ascribed to each atom, dispersion interactions, and short-range repulsion terms. Long-range Coulomb interactions are approximated by the Wolf summation method, and all interactions go to zero at interatomic spacings larger than 10 Å. To incorporate the effects of partial covalency, a Stillinger–Weber-type<sup>44</sup> three-body interaction is also applied to provide a relatively slight energetic bias toward certain atomic triplets toward certain angles. The form and parameters for the two- and three-body interactions can be found in previous work.<sup>36</sup>

**B. Systems.** Four interfacial systems were simulated: (1) a 3 nm film of water confined between two amorphous silica slabs, (2) a 3 nm diameter cylindrical pore in amorphous silica filled

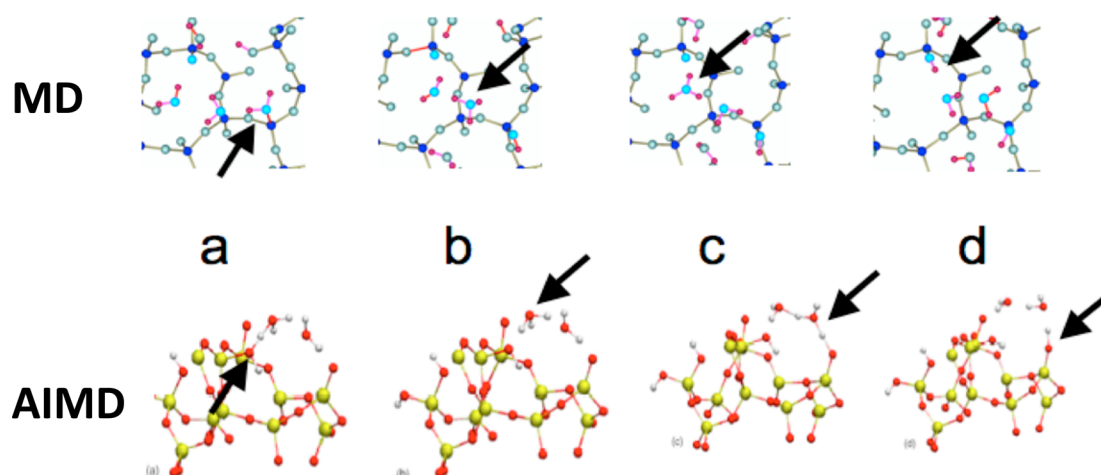


**Figure 2.** Top: Snapshots from movie of MD simulations of the amorphous silica surface exposed to water vapor.<sup>35</sup> Bottom: AIMD simulations of several water molecules adjacent to amorphous silica surface.<sup>43</sup> Arrows point to adsorption site (a), formation of  $\text{H}_3\text{O}^+$  ions and proton exchange (b, c), and deposition of proton forming second SiOH site (d).

**Table 1.** Simulated Systems' Size and Dimension ( $x_L$ ,  $y_L$ , and  $z_L$ )

system	$\text{SiO}_2$ atoms	$\text{H}_2\text{O}$ atoms	$x_L$ (Å)	$y_L$ (Å)	$z_L$ (Å)
(1) 3 nm film confined	11 668	14 553	63.64	63.82	42.64 Å of $\text{SiO}_2$ + $\sim 32$ Å of $\text{H}_2\text{O}$
(2) 3 nm pore, 0.9 g/cm <sup>3</sup>	15 960	5811	64.18	64.18	70.74
(3) 3 nm pore, 1.0 g/cm <sup>3</sup>	15 960	6261	64.18	64.18	70.74
(4) 2 nm film surface	36 678	21 900	104.4	104.4	50.09 Å $\text{SiO}_2$ + $\sim 19$ Å $\text{H}_2\text{O}$ + 85.00 Å vacuum

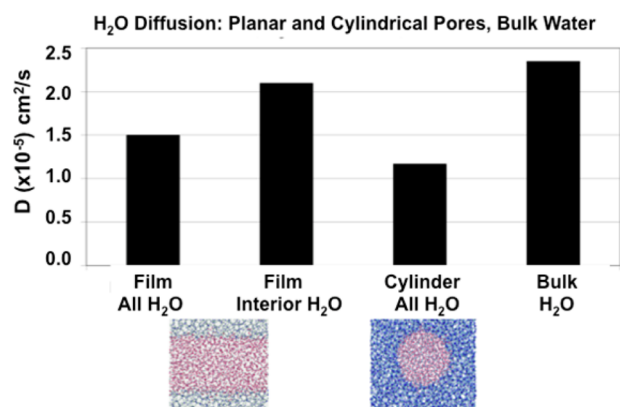


**Figure 3.** Diffusion coefficients of water in nanoconfinement in comparison to bulk water, using the diffusion of the O. "All  $\text{H}_2\text{O}$ " indicates all O from water, excluding those that attached to the silica surface to saturate coordinatively undersaturated surface Si; "Interior  $\text{H}_2\text{O}$ " indicates O within the center of volume of the film. The planar system and the cylindrical pore system used systems 1 and 3 from Table 1.

to 0.908 g/cm<sup>3</sup>  $\text{H}_2\text{O}$  density, (3) a 3 nm diameter cylindrical filled to 0.996 g/cm<sup>3</sup>  $\text{H}_2\text{O}$  density, and (4) a large silica surface covered with 2 nm of water with a vapor phase above. A summary of their dimensions is provided in Table 1. The density of water in the pore systems was determined by calculating the density within a cylinder defined by a radius of 15.25 Å from the  $x$ - $y$  center of the system and the full height of the system.

Silica glasses were first generated via a melt–quench process, annealed to minimize residual strain under constant pressure, and cut into the desired geometry while maintaining stoichiometry. Following this, the void created by the cutting

step was filled with randomly placed water molecules then allowed to equilibrate and react under constant temperature.

The melt–quench procedure is similar to that used in past simulations, where a crystal of  $\beta$ -cristobalite was melted at 6000 K and then quenched to 300 K via intermediate steps as detailed in Table 2. Each temperature step was simulated under

**Table 2.** Melt–Quench Procedure

temperature (K)	6000	4000	3000	2000	1000	300
simulation time (ps)	30	100	100	100	40	60
thermostat time (ps)	10	20	20	20	20	20

constant volume and energy (NVE), but with the first portion actively thermostated for the duration indicated. The volume *during* each step was constant, but it was adjusted *between* steps according to the thermal expansion coefficient of silica,  $5.5 \times 10^{-7} \text{ K}^{-1}$ . All four systems were generated using variations of the same five-step process shown in Table 3. NPT indicates hydrostatic pressure;  $\text{NP}_z\text{T}$  indicates only the  $z$  dimension was allowed to respond to pressure.  $r$  is the radial offset from the  $x$ - $y$  center of the system. The fill step for pore systems was done in two stages separated by a 100 ps NVT simulation because the random packing of  $\text{H}_2\text{O}$  was unable to achieve the desired densities without this intermediate condensation simulation. The resulting glasses were then annealed under a constant pressure of 101.325 kPa, and the systems' dimensions were averaged over the final half of this annealing simulation to determine their zero-strain dimensions. The final dimensions are given in Table 1.

These zero-strain glasses were then "cut" to create vacuum into which water could be inserted. This was achieved by removing stoichiometric  $\text{SiO}_2$  units to create the desired system geometry while maintaining overall neutral charge (systems 2,

Table 3. Method Used To Create Each Water–Silica Interfacial System

system	melt–quench	anneal	cut	fill	equilibration (200 ps)	production (NVE)
(1) 3 nm film confined	see Table 2	40 ps, NPT	no atoms removed	+4851 H <sub>2</sub> O	NP <sub>z</sub> T 200 ps	1.0 ns
(2) 3 nm pore 0.9 g/cm <sup>3</sup> H <sub>2</sub> O		100 ps, NP <sub>z</sub> T	$r < 15.25$ removed	+1427 H <sub>2</sub> O +550 H <sub>2</sub> O	100 ps NVT NVT 200 ps	1.0 ns
(3) 3 nm pore 1.0 g/cm <sup>3</sup> H <sub>2</sub> O		100 ps, NP <sub>z</sub> T	$r < 15.25$ removed	+1427 H <sub>2</sub> O +660 H <sub>2</sub> O	100 ps NVT NVT 200 ps	1.0 ns
(4) 2 nm film surface		40 ps, NPT	$z > 50.009$ removed	+7300 H <sub>2</sub> O	NVT 200 ps	200 ps

3, and 4) or dividing the silica in half along an arbitrary  $z$  plane and moving the top half up by 50 Å (system 1).

Water molecules were then randomly inserted into these cut silica systems such that (a) no two oxygen atoms were within 2.8 Å of each other and (b) every randomly inserted molecule was wholly within the free volume created during the cut step. Following this fill step, all atoms in all systems were randomly assigned a Gaussian velocity distribution, and then simulated under constant temperature for 200 ps to allow the randomly inserted H<sub>2</sub>O to condense and react with the silica surfaces.

Following this equilibration step, the dimensions of the confined film system (system 1) were rescaled to the average dimensions over the final half of its equilibration simulation. This procedure was unnecessary for the other three systems since they were equilibrated at constant volume. These resulting water–silica interfacial systems were simulated under constant energy for the duration indicated in Table 3, and the data presented are wholly derived from these production simulations. A time step of 0.1 fs is used throughout the simulations, providing a low energy drift of  $\sim 6 \times 10^{-4}$  kJ/mol per ps.

**C. Lifetime Calculations.** Proton autocorrelation functions, generically referred to as  $c(t)$ , are a convenient way of characterizing the lifetimes of protonated sites.<sup>2,6,9</sup> Given an oxygen with an excess proton (hereafter denoted O\*) at time  $t = 0$ ,  $c(t)$  represents the probability that that the oxygen will have an excess proton at time  $t$ . The form used here is the continuous autocorrelation function,  $c_c(t)$ , given as

$$c_c(t) = \frac{\langle h(0)H(t) \rangle}{\langle h \rangle}$$

Taking  $t = 0$  to be the time at which a given oxygen becomes O\*,  $H(t) = 1$  if the given oxygen has remained O\* continuously from time 0 to  $t$ .

This proton autocorrelation function is applied here in a fashion consistent with previous work.<sup>6</sup> Each excess H<sup>+</sup> ion is assigned a donor oxygen (labeled O<sub>d</sub>, which is its nearest neighbor and also O\* by definition) and an acceptor oxygen (labeled O<sub>a</sub>, its second-nearest oxygen neighbor), and the identity of these donor and acceptor oxygens are re-evaluated at each time step. If the identity of O<sub>a</sub> and O<sub>d</sub> switch and the distance between the H<sup>+</sup> and the new O<sub>a</sub> is greater than 1.2 Å, the proton is said to have transferred. The lifetime for the old O<sub>d</sub> is recorded, and the lifetime for the new O<sub>d</sub> begins at this instant.

To eliminate the effects of H<sub>2</sub>O (as opposed to H<sub>3</sub>O<sup>+</sup>) rattling, all transfers where the acceptor oxygen is OH<sup>-</sup> are discarded when calculating  $c(t)$ . This distinction eliminates the recombination reaction following H<sub>2</sub>O ionization rattling from skewing the lifetimes to very short durations.<sup>6</sup>

In addition,  $t = 0$  is always defined as when a given site first accepts a proton, and the only protonated sites included in the  $c(t)$  measurements presented here are those where both the

proton acceptance ( $t = 0$ ) and subsequent donation (deprotonation) are both observed within the production simulations. Cases where only one bounding limit of a site's lifetime (either the protonation or deprotonation, but not both) were observed during the production simulations were discarded. However, sites that neither protonated nor deprotonated during the entire production step (i.e., very stable protonated sites) were included; these sites simply shift all points in  $h(t)$  by a constant amount and ensure that the overall long-term stability of each site is reflected in its  $c(t)$ .

### III. RESULTS AND DISCUSSION

Figure 4 shows the different types of hydroxyls present on the silica surface exposed to water that are relevant to the work

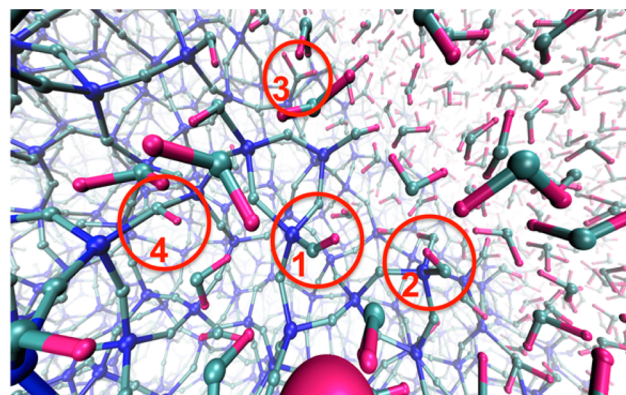


**Figure 4.** Different types of hydroxyls present on the silica surface exposed to water that are relevant to the work presented here (snapshot taken from a portion of system 3, Table 1). The site labels are as follows: 1 is an SiOH site, 2 is a geminal site, 3 is an SiOH<sub>2</sub><sup>+</sup> site, and 4 is a proton on a bridging oxygen (Si–(OH<sup>+</sup>)–Si) site.

presented here (snapshot taken from a portion of system 3, Table 1). The site labels are 1 is a silanol (SiOH) site; 2 is a geminal (Si(OH)<sub>2</sub>) site, 3 is an SiOH<sub>2</sub><sup>+</sup> site, and 4 is a proton on a bridging oxygen (Si–(OH<sup>+</sup>)–Si) site.

**A. Lifetimes in 3 nm Confined Film.** The 3 nm confined film system is the simplest case due to its lack of interfacial curvature and lack of a water–vapor interface. It has also been studied in the past<sup>17,36</sup> and provides a good baseline for interfacial phenomena. After 1.0 ns of simulation under constant energy, the final configuration in this system contained 442 SiOH, 58 bridging OH, and 6 SiOH<sub>2</sub><sup>+</sup>. Of the 442 SiOH, 134 were geminal sites (two OH's attached to a single Si, labeled Q<sup>2</sup> Si), and 5 were attached to Q<sup>1</sup> sites (Si with only 1 bridging oxygen). However, it should be noted that, throughout the 1 ns run, a total of 446 different SiOH formed, 164 different bridging OH formed, and 96 different SiOH<sub>2</sub><sup>+</sup> formed. The first set of numbers shows the number of specific hydroxyls at an instant. The second set of numbers, especially in the latter two

cases, shows that there is a significantly larger number of these transient surface sites contributing to proton diffusion throughout the run. In comparison to the number of  $\text{H}_3\text{O}^+$  at a pH of 7 for neutral water, the concentration of mobile protons is significantly enhanced by the presence of these surface sites.

These surface concentrations are within experimental expectation: the SiOH concentration corresponds to  $5.4 \text{ nm}^{-2}$  under the assumption of zero surface roughness and zero penetration (an upper limit to the true value<sup>17,45,46</sup>), and the 30% geminal population is within the range reported for silica.<sup>47</sup> While not a focus of this study, it is worthwhile to indicate that the five  $\text{Q}^1$  sites were stable throughout the 1 ns simulation and resulted from the cutting process indicated in Table 3 rather than hydrolytic reactions. No  $\text{Q}^0$  sites (silicic acid, or  $\text{Si}(\text{OH})_4$ ) ever formed during this time. Previous simulations using this potential resulted in an overall activation barrier for the formation of the  $\text{Q}^0$  from the  $\text{Q}^4$  as  $\sim 15 \text{ kcal/mol}$ ;<sup>41</sup> such a result fits within the experimentally observed range that varies from 14 to 28 kcal/mol. A population of transient  $\text{H}_3\text{O}^+$  near the interface also existed throughout the simulation of this system and is consistent with observations in molecular dynamics (MD) and quantum mechanical (QM) simulations.<sup>35,43,48</sup>

The behaviors of excess protons in solution are reasonably well-characterized from experiment<sup>5,8</sup> and simulation<sup>4,49</sup> including simulations using the model employed in this study.<sup>6,7</sup> As such, examining the lifetime distribution of  $\text{H}_3\text{O}^+$  within 6 Å (the width of the interfacial region in the core-shell concept of this flat water-silica interface<sup>17,39,40</sup>) quickly highlights the effect of the interface (Figure 5).

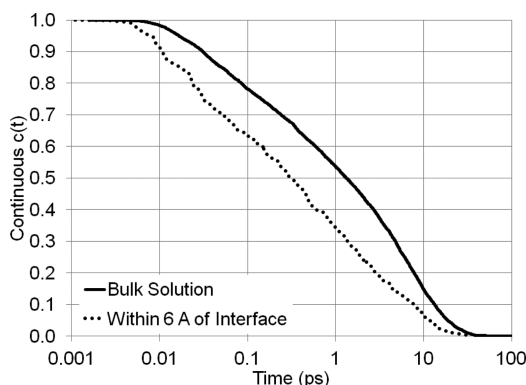


**Figure 5.** Continuous  $c_c(t)$  for  $\text{H}_3\text{O}^+$  in bulk solution<sup>6</sup> and within 6.0 Å of the water-silica interfaces in the 3 nm confined film system. These interfaces are defined to be at  $z = 21.0 \text{ Å}$  and  $z = 53.0 \text{ Å}$ .

The interface significantly shortens the mean continuous lifetime of  $\text{H}_3\text{O}^+$  from 4.5 ps in bulk solution<sup>6</sup> to 1.81 ps, and this reduced probability of continuous protonation is present at all time scales. Notably, the interface induces extremely short-lived ( $< 10 \text{ fs}$ ) hydronium ions not present in bulk solution as well as an increased deprotonation probability whose rate is nearly constant from 0.01 to 10 ps in this semilog plot. For lifetimes  $t > 3.0 \text{ ps}$ , the value of  $c_c(t)$  for hydronium ions in bulk water decreases more rapidly than  $c_c(t)$  near the interface but is always longer lived than those  $\text{H}_3\text{O}^+$  at the interface.

The  $c_c(t)$  values calculated for the other protonated sites in this 3 nm confined film system are shown in Figure 6. All sites of excess charge,  $\text{SiOH}_2^+$ , interfacial  $\text{H}_3\text{O}^+$ , and  $\text{Si}-(\text{OH}^+)-\text{Si}$ ,

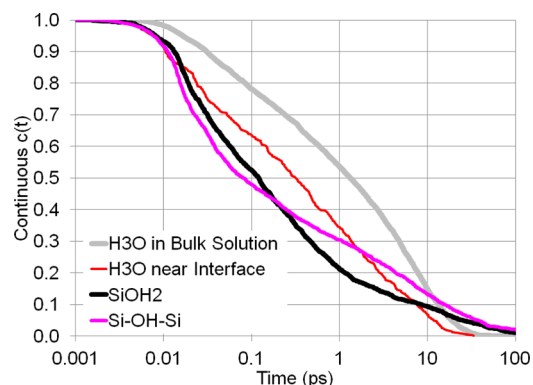


**Figure 6.** Comparison of continuous autocorrelation functions for sites of excess charge at the water-silica interface in the 3 nm film.  $\text{H}_3\text{O}^+$  in bulk solution also included for comparison.

show lifetime probabilities with very similar behavior, and all of these sites exhibit considerably greater probabilities of subpicosecond lifetimes than  $\text{H}_3\text{O}^+$  in bulk solution and in the absence of interfacial effects. The two protonated sites attached to the  $\text{SiO}_2$  network,  $\text{SiOH}_2^+$  and  $\text{Si}-(\text{OH}^+)-\text{Si}$ , also show inflections in  $c_c(t)$  around a precipitous drop in protonation probability between  $t = 0.010 \text{ ps}$  and  $t = 0.100 \text{ ps}$ . In addition, these two sites exhibit a small but finite probability of very long lifetimes ( $t > 100 \text{ ps}$ ); neither the inflections nor the long-lived tails are present for  $\text{H}_3\text{O}^+$  and suggest behavior unique to the far less-mobile Si-O sites.

On the other hand, SiOH is considerably more stable, and only a fraction of all SiOH sites (14.3% in the 3 nm confined film) ever show the capacity to deprotonate during the 1.0 ns production step. A significant majority of this 14.3% of “reactive SiOH sites” deprotonate to bridging oxygen (see second column of Table 4) as the result of SiOH forming very close to an existing bridging oxygen ( $r_{\text{OO}} < 2.55 \text{ Å}$ ), creating the unstable SiOH site as a result. However, such a site not only deprotonates but also reprotonates.

**C. Effect of Curvature.** The  $c_c(t)$  for each protonated site in all four simulated systems listed in Table 3 is shown in Figure 7.

In the case of  $\text{H}_3\text{O}^+$  near the interface, all systems exhibit  $c_c(t)$  shifted toward shorter lifetimes relative to the case of  $\text{H}_3\text{O}^+$  in solution. However, the flat systems, noted by red (confined) and dashed blue (surface film) lines, show a slightly greater tendency to longer lifetimes than the pore systems (thin black and magenta lines) for  $t > 30 \text{ fs}$ . Given that the effect of the interface is to shift  $c_c(t)$  to shorter lifetimes, this difference due to curvature may be a simple effect of the interfacial region being represented here ( $9.25 \text{ Å} < r < 15.25 \text{ Å}$ , where  $r$  is the radial distance from the center of the pore) having a larger volume closer to the interface (e.g.,  $12.25 \text{ Å} < r < 15.25 \text{ Å}$ ) than farther away ( $9.25 \text{ Å} < r < 12.25 \text{ Å}$ ).

The behavior of  $\text{Si}-(\text{OH}^+)-\text{Si}$ , on the other hand, shows very similar behavior in the cylindrical pores while the two planar systems are more divergent (Figure 7). Because this site is dependent upon the atomic connectivity of the silica surface on which it forms, the similarities between the two cylindrical systems (which share the same original silica matrix) are anticipated. However, the two planar interface systems show no clear trend toward longer or shorter protonation lifetimes with respect to the curved interfaces; thus, it is likely that the lifetimes of  $\text{Si}-(\text{OH}^+)-\text{Si}$  are more dependent upon the actual

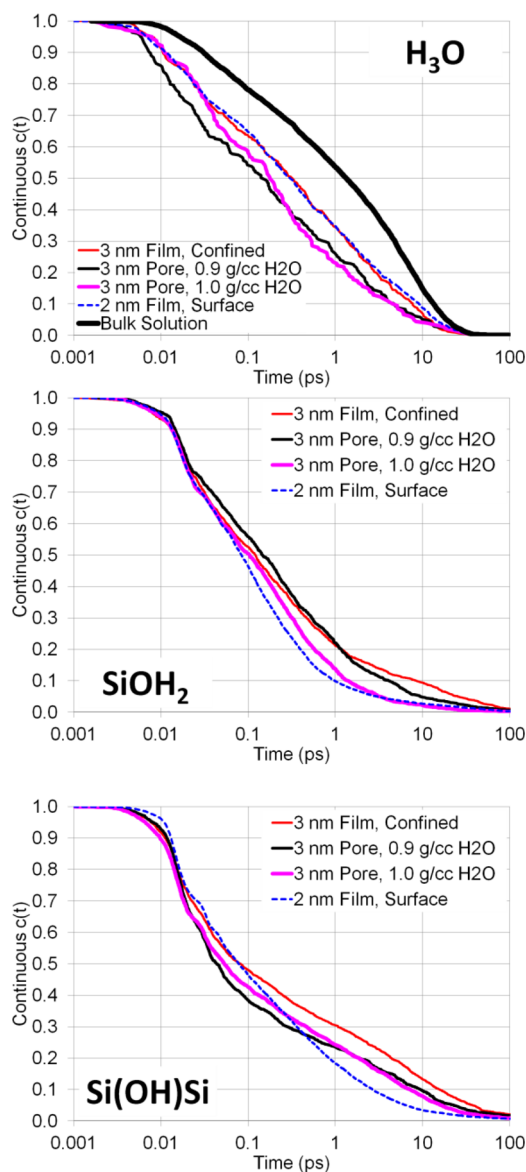


**Figure 7.** Continuous  $c_c(t)$  for  $\text{H}_3\text{O}^+$ ,  $\text{SiOH}_2^+$ , and  $\text{Si}-(\text{OH}^+)-\text{Si}$  sites in the four simulated systems (3 nm confined film, 3 nm cylindrical pore filled with  $0.9 \text{ g/cm}^3 \text{ H}_2\text{O}$ ,  $1.0 \text{ g/cm}^3 \text{ H}_2\text{O}$ , and 2 nm film on a silica surface).

features of the surface (localized roughness, pits, and channels, etc.) than overall curvature or mesoscale topography, as discussed below.

$\text{SiOH}_2^+$  sites show less clear trends in  $c_c(t)$  with respect to surface curvature: the confined film and low-density pore show similar  $c_c(t)$ , and the surface film and high-density pore also show similar  $c_c(t)$ . However, these two pairs of systems show some divergence in the broad range of  $10^{-1} < t < 10^1$  ps, with the  $1.0 \text{ g/cm}^3$  pore and 2 nm surface film showing increased tendencies to deprotonate for  $t > 100$  fs.

As with the confined 3 nm film, the majority of  $\text{SiOH}$  never deprotonated in the cylindrical systems. However, the fraction of reactive sites (those that exhibited any deprotonation) increased from 14.3% and 15.4% in the confined and surface films to 19.5% and 21.5% in the  $0.9 \text{ g/cm}^3$  pore and  $1.0 \text{ g/cm}^3$  pore, respectively. The geometry of cutting a curved interface from the silica network results in a greater number of closely spaced silica  $\text{O}-\text{O}$  in contact with water as well as a greater

number of nonbridging oxygen before the glass is even exposed to water. As shown in Table 4, this difference in surface structure results in a smaller fraction of  $\text{SiOH}$  sites donating to bridges and a larger fraction donating to nonbridging oxygen.

**D. Effect of Subsurface Depth on Lifetimes.** It is convenient to divide the flat systems into slices in  $z$  to ascertain whether the depth at which these sites exist below the silica surface is causing the wide range of lifetimes exhibited. Because the 2 nm surface film system has the largest surface area of the four systems simulated and a very well-defined interface at  $z = 50.009 \text{ \AA}$  (the location at which the  $\text{SiO}_2$  was cut during the Cut step of system assembly), the results of this depth analysis presented here are from that system. However, the same analysis was performed on the 3 nm confined film system, and the results were similar.

In the case of  $\text{SiOH}_2^+$  (Figure 8a),  $\text{SiOH}_2^+$  species protruding into the water [“above the surface”, or  $+3 \text{ \AA} > (dz = z_i -$

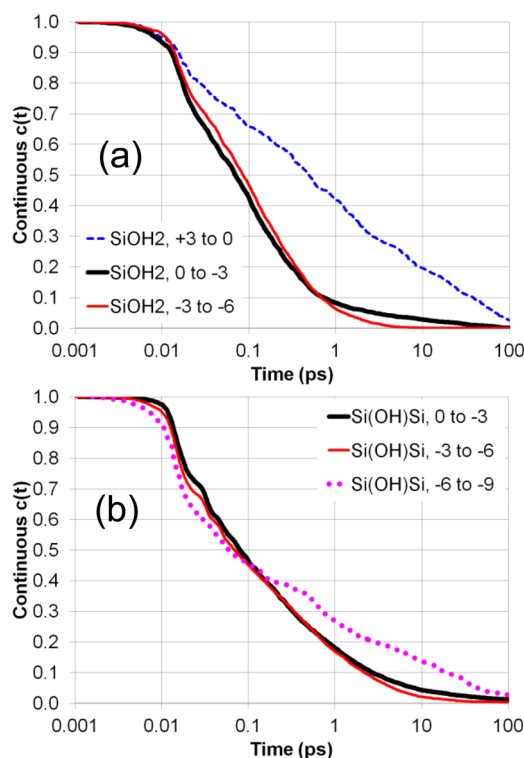


**Figure 8.**  $c_c(t)$  of (a)  $\text{SiOH}_2^+$  and (b)  $\text{Si}-(\text{OH}^+)-\text{Si}$  sites in the 2 nm surface film system as a function of subsurface depth. The surface was cut at  $z = 50.0 \text{ \AA}$ , so “+3 to 0” corresponds to a volume element bounded by  $50.0 \text{ \AA} < z < 53.0 \text{ \AA}$ , “0 to -3” is  $47.0 \text{ \AA} < z < 50.0 \text{ \AA}$ , and “-3 to -6” is  $44.0 \text{ \AA} < z < 47.0 \text{ \AA}$ .

$z_{\text{interface}}) > +0 \text{ \AA}$  above the interface, where  $z_i$  is the  $z$  location of the O] tend to retain protons for longer times than  $\text{SiOH}_2^+$  sites “at the surface” ( $+0 \text{ \AA} > dz > -3 \text{ \AA}$ ) and “below the surface” ( $-3 \text{ \AA} > dz > -6 \text{ \AA}$ ). While all types are unstable in comparison the  $\text{H}_3\text{O}^+$  in water, the results indicate that subsurface  $\text{SiOH}_2^+$  are far less stable than  $\text{SiOH}_2^+$  that are sticking above the surface. As will be discussed below regarding proton transfer, the key differentiating factor between the above-surface and at- or below-surface volumes is the presence of the silica network for the latter group. The presence of neighboring O in the silica network at a close distance allows for rapid and short-lived rattling of the proton between donor

and acceptor sites, causing the rapid decrease in the  $\text{SiOH}_2^+$  species at  $dz < 0 \text{ \AA}$ .

$\text{Si}-(\text{OH}^+)-\text{Si}$  does not exist above the interface (i.e., the  $z$ -plane above which all silica atoms, including all bridging oxygens, were removed). As shown in Figure 8b, these sites show a median time to deprotonation between 64 fs ( $-3 \text{ \AA} > dz > -6 \text{ \AA}$  depth) to 99 fs ( $+0 \text{ \AA} > dz > -3 \text{ \AA}$ ). By comparison,  $c_c(t)$  for  $\text{SiOH}_2^+$  shows a median time to deprotonation of between 67 fs ( $+0 \text{ \AA} > dz > -3 \text{ \AA}$ ) and 100 fs ( $-3 \text{ \AA} > dz > -6 \text{ \AA}$ ).

Unlike  $\text{SiOH}_2^+$ , though,  $\text{Si}-(\text{OH}^+)-\text{Si}$  occurs at subsurface depths between  $-6 \text{ \AA} > dz > -9 \text{ \AA}$  where no  $\text{SiOH}_2^+$  is ever present, and these bridges show an appreciably higher tendency to remain protonated for lifetimes  $t > 0.1$  ps. Because of the absence of any other protonated sites at these depths, the deprotonations contributing to  $c_c(t)$  in this case must be bridge-to-bridge transfers. Previous work has shown that protons preferentially bind to strained bridges with  $\text{Si}-\text{O}-\text{Si}$  angles of  $\sim 135^\circ$ ,<sup>36,50,51</sup> and it is likely that the two lifetime populations within  $-6 \text{ \AA} > dz > -9 \text{ \AA}$  (those with lifetimes  $t < 0.1$  and  $0.1 \text{ ps} < t < 50 \text{ ps}$ ) are the result of protons either rapidly rattling between bridges with angles not favorable for proton adsorption (bridges with angles greater than  $\sim 140^\circ$ ) or stably adsorbing to strained bridges ( $\sim 135^\circ$ ) and exhibiting limited mobility (deprotonation) thereafter.

**E. Subsurface Proton Transfer Mechanisms.** While the subsurface protonated sites are not expected to play an important role in the high proton conductivity in electrochemical studies mentioned above because of their low concentration, they are nonetheless worth discussing because of their possible role in proton migration inside silica. The subsurface region in the silica matrix provides for both very short protonation lifetimes on the hydroxylated sites as well as very long lifetimes for a small number of both  $\text{SiOH}_2^+$  and  $\text{Si}-(\text{OH}^+)-\text{Si}$ . The former sites involve local rattling between a closely spaced donor and acceptor, whereas the latter sites tend to exist in parts of the silica subsurface where there is no acceptor site within a close enough distance for deprotonation to occur. An example where proton exchange occurs between an  $\text{SiOH}_2^+$  and an adjacent bridge is shown in Figure 9. Here an  $\sim 9 \text{ \AA}$  pit in the silica surface, formed during the melt-quench process, allowed a water molecule to migrate to a 3-coordinated Si at site C, enabling the formation of a  $\text{SiOH}_2^+$  upon an initial nondissociative chemisorption. The presence of the nearby bridging oxygen in the silica network (site B) then facilitated deprotonation and formation of the  $\text{Si}-(\text{OH}^+)-\text{Si}$  (at B) and  $\text{SiOH}$  (at A) shown in the figure.

Starting from the two hydroxyls in Figure 9, the plot of the two OH distances and  $\text{SiOSi}$  angle in the figure shows the transfer of the proton from B back to A at  $\sim 823$  ps, reforming the initial  $\text{SiOH}_2^+$ , with the back reaction at  $\sim 827$  ps. Despite being embedded in the silica network, the  $\text{Si}-(\text{OH}^+)-\text{Si}$  angle shows some flexibility while protonated ( $t < 823.0$  ps). The lowest angles experienced before transfer ( $\sim 136^\circ$ ) are near the range of preferred angles for proton adsorption, but the widest angles ( $\sim 146^\circ$ ) are an unstable angle for adsorption.<sup>36</sup> Of course, the  $\sim 146^\circ$  angle is close to the average value for amorphous silica observed experimentally ( $146^\circ-150^\circ$ ). Despite vibrating to these wider angles virtually every picosecond, they alone do not guarantee proton transfer to the  $\text{SiO}_A\text{H}$  site. This is similar to proton transfer in the Zundel complex in bulk water, where the barrier to proton transfer from hydronium oxygen to an acceptor oxygen decreases with

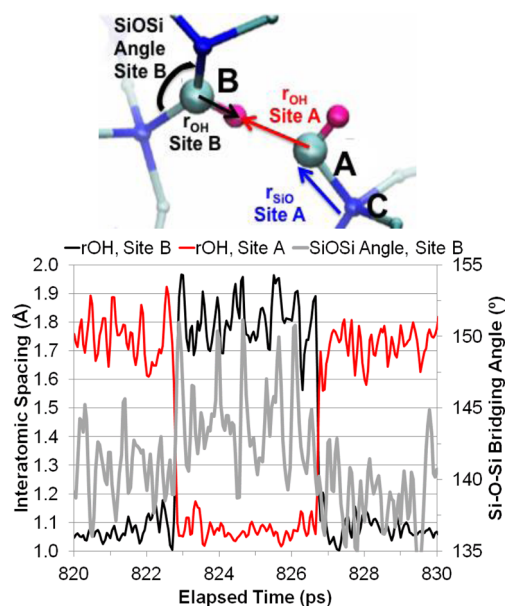


**Figure 9.** Site A is a  $\text{SiOH}$  and Site B a  $\text{Si}-(\text{OH}^+)-\text{Si}$ ; these two sites formed as the result of the dissociative chemisorption of a water molecule at site C which originated as a 3-coordinated Si. Atom B is the bridging oxygen, and atom A is the nonbridging oxygen.  $r_{\text{O-H}}$  is the O-H distance between oxygen and the excess proton at sites A and B,  $r_{\text{Si-O}}$  is the distance between oxygen A and its neighbor Si used in Figure 10, and  $r_{\text{A-B}}$  is the oxygen-oxygen distance used in Figure 10

decreasing acceptor-donor oxygen spacing. This relation between decreased barrier to decreased spacing was similarly observed in simulations of water.<sup>6</sup>

The bonding environment labeled in Figure 9 is examined immediately before the successful transfer from site B to site A every 50 fs and is shown in Figure 10. The results reveal that

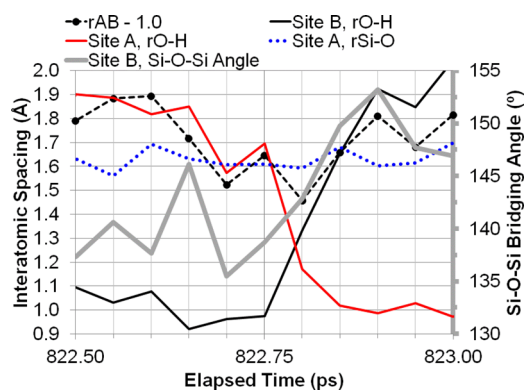


**Figure 10.** Geometry during transfer from bridge to  $\text{SiOH}$ . The O-O spacing,  $r_{\text{AB}}$ , is represented above as  $(r_{\text{AB}} - 1.0 \text{ \AA})$ .

the transfer is coincident with a widening of the bridging angle (thick gray line), but the transfer of  $\text{H}^+$  from  $\text{O}_B$  to  $\text{O}_A$  (solid black and red lines, respectively) between  $t = 822.75$  ps and  $t = 822.85$  ps also occurs as the  $\text{O}_A-\text{O}_B$  spacing (dashed line generated as  $r_{\text{AB}} - 1$  to fit on this figure) falls below  $2.5 \text{ \AA}$  at  $822.80$  ps. This O-O distance is below that at which proton transfer between  $\text{H}_3\text{O}^+$  and  $\text{H}_2\text{O}$  is observed in liquid water.<sup>6</sup> This narrowing of  $\text{O}_A-\text{O}_B$  is not caused by the  $\text{Si}-\text{O}_A$  distance increasing, though; this  $\text{Si}-\text{O}_A$  distance (dotted blue line) is quite stable throughout the transfer process.

From this, it is clear that the transfer of  $H^+$  from  $O_B$  to  $O_A$  is initiated by a narrowing of the  $O_A-O_B$  spacing concurrent with a widening of the  $Si-O_B-Si$  angle. This  $O_A-O_B$  distance is narrowing despite both the  $Si-O_A$  bond not stretching and the  $Si-O_B-Si$  angle actually widening. This is possible via some medium-range collective motion within the local rings in the silica network where the entire  $SiO_AH$  and  $Si-(O_BH^+)-Si$  complexes are moving toward each other in a breathing-like vibration mode. The widening of the  $Si-(O_BH^+)-Si$  raises the energy of the adsorbed  $H^+$ , and the reduced  $O_A-O_B$  distance reduces the activation barrier to transfer so that the proton transfers and forms  $SiOH_2^+$ . This site persists for 4 ps before both the  $O_A-O_B$  distance is short enough and the  $Si-(O_BH^+)-Si$  angle narrow enough for the reverse reaction to occur.

The amorphous nature of the silica also makes the environment surrounding each metastably adsorbed subsurface proton prone to different localized breathing modes that moderate the frequency of these transfers. In fact, the simulated systems all exhibit a small number of subsurface sites with equilibrium  $O_A-O_B$  spacing near 2.5 Å, and by virtue of the fact that these sites spend a significant amount of time with  $r_{AB} < 2.5$  Å, the proton transfers back and forth repeatedly throughout the entire 1.0 ns production runs. Thus, the short-time portions of  $c_c(t)$  for  $SiOH_2^+$  and  $Si-(OH^+)-Si$  are composed of rapid  $H^+$  transfers between unstable subsurface sites analogous to “proton rattling” observed in water.

Once adsorbed to a metastable subsurface site, both  $SiOH_2^+$  and  $Si-(OH^+)-Si$  have the capacity to exhibit long lifetimes. These can occur when there is not an acceptor site sufficiently close to the adsorption site, preventing proton transfer, thus creating these long lifetimes observed in  $c_c(t)$  for these two sites.

An analogous tail is not present in the  $H_3O^+$   $c_c(t)$  as a result of its mobility. While proton transfer from  $H_3O^+$  molecules does involve the concerted motions of molecules in the hydronium ion's second solvation shell,<sup>6,49</sup> the connectivity of the hydrogen bond network is far less rigid than that of the silica network, allowing the necessary geometric criteria for transfer to occur much more frequently. It follows that proton transport in regions in contact with the hydrogen bond network will be faster than proton transport in the interior of the bulk silica network, and this is consistent with the observation of enhanced proton conduction in hydrated high-surface area silicas but not low-surface area nonporous silica.<sup>52-54</sup>

**F. Implications for Proton Conduction.** Proton transfer via hydronium ions was the assumed mechanism used to explain the high proton conductivity in wet mesoporous silica.<sup>55-57</sup> The current and previous<sup>35</sup> simulations show the formation of excess  $H_3O^+$  at the water/silica interface; formation of the hydronium ion at the interface is also observed in ab initio calculations.<sup>43,48</sup> More importantly, the current simulations indicate that those  $H_3O^+$  ions near the interface have much shorter lifetimes than those in bulk water. An earlier study of the  $Si-(OH^+)-Si$  site suggests that it can also act as a pathway for proton conduction along the surface.<sup>36</sup> Considering the third short-lifetime site,  $SiOH_2^+$ , and the similarities in lifetime populations shown in Figure 6, it follows that all three sites of excess charge can contribute to proton transport along the water-silica interface.

Furthermore, the majority of proton transfers observed in all systems occur in the immediate vicinity of the interface. Figure 11 provides the sites to which the interfacial  $H_3O^+$ , the

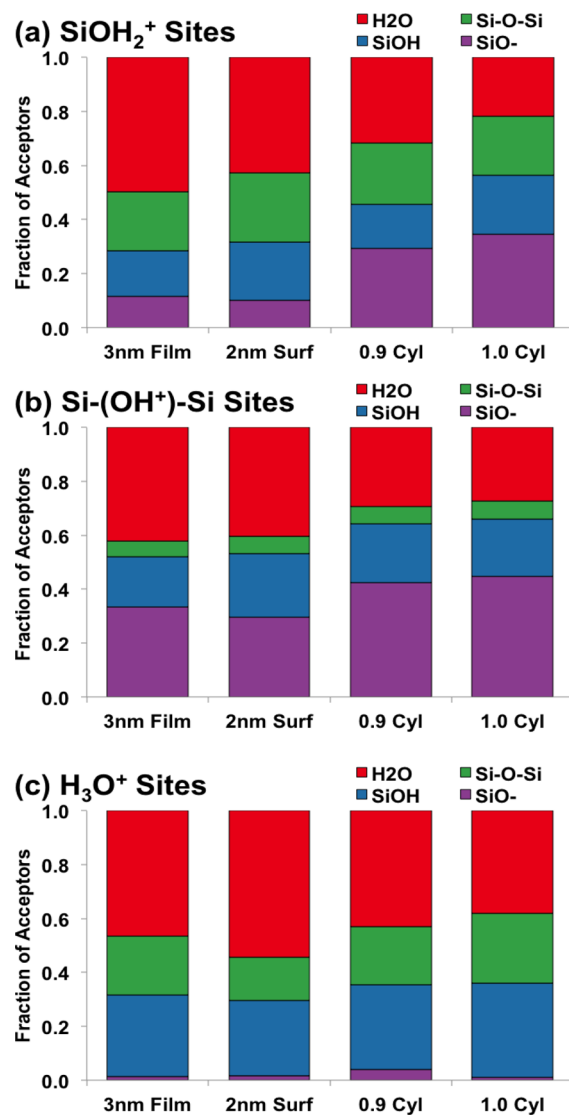


**Figure 11.** Distribution of acceptor sites receiving protons from (a)  $SiOH_2^+$  sites, (b)  $Si-(OH^+)-Si$  sites, and (c)  $H_3O^+$ . Alternatively, these data express the probability that any given site will donate its proton to the given acceptor.

$SiOH_2^+$ , and the  $Si-(OH^+)-Si$  donate their excess proton. Figure 11a,b reveals that  $H_2O$  is the significantly predominant acceptor (forming  $H_3O^+$ ) in both planar systems and less so in the cylindrical systems for  $SiOH_2^+$  and  $Si-(OH^+)-Si$ . Proton transfers from the  $H_3O^+$  ion to  $H_2O$  molecules are dominant for this protonated site (Figure 11c), but there is also significant transfer to the two surface excess charge sites. These surface sites are similarly unstable and provide additional pathways for rapid proton transport.

Anhydrous nonbridging sites ( $SiO^-$ ) appear to play a negligible role in proton mobility near the interface, as these sites form the  $SiOH$  site that is highly stable against deprotonation. The overall concentration of  $SiO^-$  near the water is extremely low as a result of the propensity for these sites to stably adsorb  $H^+$ ; those  $SiO^-$  sites that formed after the Cut step simply hydrated quickly to become  $SiOH$ . Protons reaching such sites that may exist subsurface also become stable  $SiOH$ .

Therefore, Figure 11a,b indicates formation of such terminating  $SiOH$  sites for the  $SiOH_2^+$  and  $Si-(OH^+)-Si$

donors, although a strong majority of the acceptor sites for these donors (over ~60%) form the unstable excess charge species which are both surface and subsurface sites. While the subsurface sites are not expected to make much of a contribution to the overall proton conductivity that is dominated by the interface (surface) behavior, the subsurface sites create protons that are certainly weakly bound and rattling between these adjacent sites. This makes these protons more likely to migrate over time

#### IV. CONCLUSIONS

The heterogeneity of the amorphous silica surface provides a number of active sites to which excess  $H^+$  can transiently adsorb, creating shorter lifetimes than hydrated protons in water ( $H_3O^+$  ion in bulk water). Such sites provide additional mechanisms by which proton migration can proceed and proton conduction is enhanced in amorphous silica exposed to water. Even  $H_3O^+$  ions adjacent to the silica surface show shorter lifetimes than those in bulk water.  $SiOH_2^+$ ,  $Si-(OH^+)-Si$ , and  $H_3O^+$  all participate in the rapid proton transfer at the water-silica interface, providing the molecular mechanisms for the increased proton transport in wet mesoporous silica observed in electrochemical studies. The simulations show that differences in atomistic topography such as curvature and roughness will affect the overall lifetime of protons on these various sites. Subsurface protons were also observed to have distinctly bimodal lifetimes as a result of the differences in local structure that affect the proton's ability to sample favorable hopping sites. As a result, they generally either rattle between neighboring oxygens or are very long-lived, with deprotonation of the latter type only being possible when collective breathing of the local silica network reduces the donor-acceptor oxygen spacing enough to make the proton transfer energetically favorable.

#### AUTHOR INFORMATION

##### Corresponding Author

\*E-mail: shg@rutgers.edu.

##### Notes

The authors declare no competing financial interest.

#### REFERENCES

- (1) Tuckerman, M.; Laasonen, K.; Sprik, M.; Parrinello, M. Ab-initio molecular dynamics simulation of the solvation and transport of  $H_3O^+$  and  $OH^-$  ions in water. *J. Phys. Chem.* **1995**, *99*, 5749–5752.
- (2) Markovitch, O.; Chen, H.; Izvekov, S.; Paesani, F.; Voth, G. A.; Agmon, N. Special pair dance and partner selection: Elementary steps in proton transport in liquid water. *J. Phys. Chem. B* **2008**, *112*, 9456–9466.
- (3) Wu, Y.; Chen, H.; Wang, F.; Paesani, F.; Voth, G. A. An improved multistate empirical valence bond model for aqueous proton solvation and transport. *J. Phys. Chem. B* **2008**, *112*, 467–482.
- (4) Chen, H.; Voth, G. A.; Agmon, N. Kinetics of proton migration in liquid water. *J. Phys. Chem. B* **2010**, *114*, 333–339.
- (5) Woutersen, S.; Bakker, H. J. Ultrafast vibrational and structural dynamics of the protons in liquid water. *Phys. Rev. Lett.* **2006**, *96*, 138305.
- (6) Lockwood, G. K.; Garofalini, S. H. Lifetimes of excess protons in water using a dissociative water potential. *J. Phys. Chem. B* **2013**, *117*, 4089–4097.
- (7) Hofer, T.; Hitznerberger, M.; Randolf, B. Combining a dissociative water model with a hybrid QM/MM approach-A simulation strategy for the study of proton transfer reactions in solution. *J. Chem. Theory Comput.* **2012**, *8*, 3586–3595.
- (8) Luz, Z.; Meiboom, S. The activation energies of proton transfer reactions in water. *J. Am. Chem. Soc.* **1964**, *86*, 4768–4769.
- (9) Chandra, A.; Tuckerman, M. E.; Marx, D. Connecting solvation shell structure to proton transport kinetics in hydrogen-bonded networks via population correlation functions. *Phys. Rev. Lett.* **2007**, *99*, 145901.
- (10) Berkelbach, T. C.; Lee, H.-S.; Tuckerman, M. E. Concerted hydrogen-bond dynamics in the transport mechanism of the hydrated proton: a first-principles molecular dynamics study. *Phys. Rev. Lett.* **2009**, *103*, 238302.
- (11) Lapid, H.; Agmon, N.; Petersen, M. K.; Voth, G. A. A bond-order analysis of the mechanism for hydrated proton mobility in liquid water. *J. Chem. Phys.* **2005**, *122*, 014506.
- (12) Tielrooij, K. J.; Timmer, R. L. A.; Bakker, H. J.; Bonn, M. Structure dynamics of the proton in liquid water probed with terahertz time-domain spectroscopy. *Phys. Rev. Lett.* **2009**, *102*, 198303.
- (13) Soper, A. K.; Bruni, F.; Ricci, M. A. Water confined in Vycor glass. II. Excluded volume effects on the radial distribution functions. *J. Chem. Phys.* **1998**, *109*, 1486–1494.
- (14) Hartnig, C.; Witschel, W.; Spohr, E.; Gallo, P.; Ricci, M. A.; Rovere, M. Modifications of the hydrogen bond network of liquid water in a cylindrical  $SiO_2$  pore. *J. Mol. Liq.* **2000**, *85*, 127–137.
- (15) Sovago, M.; Campen, R. K.; Bakker, H. J.; Bonn, M. Hydrogen bonding strength of interfacial water determined with surface sum-frequency generation. *Chem. Phys. Lett.* **2009**, *470*, 7–12.
- (16) Kumar, P.; Han, S.; Stanley, H. E. Anomalies of water and hydrogen bond dynamics in hydrophobic nanoconfinement. *J. Phys.: Condens. Matter* **2009**, *21*, 504108.
- (17) Garofalini, S. H.; Mahadevan, T. S.; Xu, S.; Scherer, G. W. Molecular mechanisms causing anomalously high thermal expansion of nanoconfined water. *ChemPhysChem* **2008**, *9*, 1997–2001.
- (18) Casey, W. H.; Lasaga, A. C.; Gibbs, G. V. Mechanisms of silica dissolution as inferred from the kinetic isotope effect. *Geochim. Cosmochim. Acta* **1990**, *54*, 3369–3378.
- (19) Xiao, Y.; Lasaga, A. C. Ab initio quantum mechanical studies of the kinetics and mechanisms of silicate dissolution:  $H^+(H_3O^+)$  catalysis. *Geochim. Cosmochim. Acta* **1994**, *58*, 5379–5400.
- (20) Pelmenchikov, A.; Strandh, H.; Pettersson, L. G. M.; Leszczynski, J. Lattice resistance to hydrolysis of Si-O-Si bonds of silicate minerals: ab initio calculations of a single water attack onto the (001) and (111) beta-cristobalite surfaces. *J. Phys. Chem. B* **2000**, *104*, 5779–5783.
- (21) Criscenti, L. J.; Kubicki, J. D.; Brantley, S. L. Silicate glass and mineral dissolution: calculated reaction paths and activation energies for hydrolysis of a Q3 Si by  $H_3O^+$  using ab initio methods. *J. Phys. Chem. A* **2006**, *110*, 198–206.
- (22) Nogami, M.; Matsushita, H.; Goto, Y.; Kasuga, T. A sol-gel-derived glass as a fuel cell electrolyte. *Adv. Mater.* **2000**, *12*, 1370–1372.
- (23) Malavasi, L.; Fisher, C. A. J.; Islam, M. S. Oxide-ion and proton conducting electrolyte materials for clean energy applications: Structural and mechanistic features. *Chem. Soc. Rev.* **2010**, *39*, 4370–4387.
- (24) Maciel, G. E.; Sindorf, D. W. Silicon-29 nuclear magnetic resonance study of the surface of silica gel by cross polarization and magic-angle spinning. *J. Am. Chem. Soc.* **1980**, *102*, 7606–7607.
- (25) Sindorf, D. W.; Maciel, E. 29Si NMR study of dehydrated/rehydrated silica gel using cross polarization and magic-angle spinning. *J. Am. Chem. Soc.* **1983**, *105*, 1487–1493.
- (26) Chuang, I.-S.; Maciel, G. E. Probing hydrogen bonding and the local environment of silanols on silica surface via nuclear spin cross polarization dynamics. *J. Am. Chem. Soc.* **1996**, *118*, 401–406.
- (27) Murray, D. K. Differentiating and characterizing geminal silanols in silicas by 29Si NMR spectroscopy. *J. Colloid Interface Sci.* **2010**, *352*, 163–170.
- (28) Ong, S.; Zhao, X.; Eissenthal, K. B. Polarization of water molecules at a charged interface: second harmonic studies of the silica/water interface. *Chem. Phys. Lett.* **1992**, *191*, 327–335.

- (29) Gong, X.; Li, J.; Lu, H.; Wan, R.; Li, J.; Hu, J.; Fang, H. A charge-driven molecular water pump. *Nat. Nanotechnol.* **2007**, *2*, 709–712.
- (30) Weber, W. J.; Ewing, R. C.; Catlow, C. R. A.; Diaz de la Rubia, T.; Hobbs, L. W.; Kinoshita, C.; Matzke, H.; Motta, A. T.; Nastasi, M.; Salje, E. K. H.; Vance, E. R.; Zinkle, S. J. Radiation effects in crystalline ceramics for the immobilization of high-level nuclear waste and plutonium. *J. Mater. Res.* **1998**, *13*, 1434–1484.
- (31) Fisk, J. D.; Batten, R.; Jones, G.; O'Reilly, J. P.; Shaw, A. M. pH dependence of the crystal violet adsorption isotherm at the silica-water interface. *J. Phys. Chem. B* **2005**, *109*, 14475–14480.
- (32) Rosenholm, J. M.; Czuryzskiewicz, T.; Kleitz, F.; Rosenholm, J. B.; Lindén, M. On the nature of the Brønsted acidic groups on native and functionalized mesoporous siliceous SBA-15 as studied by benzylamine adsorption from solution. *Langmuir* **2007**, *23*, 4315–4323.
- (33) Duval, Y.; Mielczarski, J. A.; Pokrovsky, O. S.; Mielczarske, E.; Ehrhardt, J. J. Evidence of the existence of three types of species at the quartz-aqueous solution interface at pH 0–10: XPS surface group quantification and surface complexation modeling. *J. Phys. Chem. B* **2002**, *106*, 2937–2945.
- (34) Bergna, H. E., Colloid chemistry of silica: An overview. In *The Colloid Chemistry of Silica*; Bergna, H. E., Ed American Chemical Society: Columbus, OH, 1994; pp 1–47.
- (35) Mahadevan, T. S.; Garofalini, S. H. Dissociative chemisorption of water onto silica surfaces and formation of hydronium ions. *J. Phys. Chem. C* **2008**, *112*, 1507–1515.
- (36) Lockwood, G. K.; Garofalini, S. H. Bridging oxygen as a site for proton adsorption on the vitreous silica surface. *J. Chem. Phys.* **2009**, *131*, 074703.
- (37) Bandura, A. V.; Kubicki, J. D.; Sofo, J. O. Periodic density functional theory study of water adsorption on the  $\alpha$ -Quartz (101) surface. *J. Phys. Chem. C* **2011**, *115*, 5756–5766.
- (38) Mahadevan, T. S.; Garofalini, S. H. Dissociative water potential for molecular dynamics simulations. *J. Phys. Chem. B* **2007**, *111*, 8919–8927.
- (39) Xu, S.; Scherer, G. W.; Mahadevan, T. S.; Garofalini, S. H. Thermal expansion of confined water. *Langmuir* **2009**, *25*, 5076–5083.
- (40) Xu, S.; Simmons, G. C.; Mahadevan, T. S.; Scherer, G. W.; Garofalini, S. H.; Pacheco, C. Transport of water in small pores. *Langmuir* **2009**, *25*, 5084–5090.
- (41) Kagan, M.; Lockwood, G. K.; Garofalini, S. H. Simulation of the activation barrier for dissolution of amorphous silica in water using a reactive potential. *Phys. Chem. Chem. Phys.* **2014**, *16*, 9294–9301.
- (42) Marx, D.; Tuckerman, M. E.; Parrinello, M. Solvated excess protons in water: Quantum effects on the hydration structure. *J. Phys.: Condens. Matter* **2000**, *12*, A153–A159.
- (43) Ma, Y.; Foster, A. S.; Nieminen, R. M. Reactions and clustering of water with silica surface. *J. Chem. Phys.* **2005**, *122*.
- (44) Stillinger, F. H.; Weber, T. A. Computer simulation of local order in condensed phases of silicon. *Phys. Rev. B* **1985**, *31*, 5262–5271.
- (45) Zhuravlev, L. T. Concentration of hydroxyl groups on the surface of amorphous silicas. *Langmuir* **1987**, *3*, 316–318.
- (46) Bourg, I. C.; Steefel, C. I. Molecular dynamics simulations of water structure and diffusion in silica nanopores. *J. Phys. Chem. C* **2012**, *116*, 11556–11564.
- (47) Liu, C. C.; Maciel, G. E. The fumed silica surface: A study by NMR. *J. Am. Chem. Soc.* **1996**, *118*, 5103–5119.
- (48) Adeagbo, W. A.; Doltsinis, N. L.; Klevakina, K.; Renner, J. Transport processes at alpha-quartz-water interfaces: Insights from first-principles molecular dynamics simulations. *ChemPhysChem* **2008**, *9*, 994–1002.
- (49) Marx, D.; Tuckerman, M. E.; Hutter, J.; Parrinello, M. The nature of the hydrated excess proton in water. *Nature* **1999**, *397*, 601–604.
- (50) Vanheusden, K.; Korambath, P. P.; Kurtz, H. A.; Karna, S. P.; Fleetwood, D. M.; Shedd, W. M.; Pugh, R. D. The effect of near-interface network strain on proton trapping in SiO<sub>2</sub>. *IEEE Trans. Nucl. Sci.* **1999**, *46*, 1562–1567.
- (51) Geisinger, K. L.; Gibbs, G. V.; Navrotsky, A. A molecular orbital study of bond length and angle variations in framework structures. *Phys. Chem. Miner.* **1985**, *11*, 266–283.
- (52) Daiko, Y.; Kasuga, T.; Nogami, M. Proton conduction and pore structure in sol-gel glasses. *Chem. Mater.* **2002**, *14*, 4624–4627.
- (53) Daiko, Y.; Kasuga, T.; Nogami, M. Pore size effect on proton transfer in sol-gel porous silica glasses. *Microporous Mesoporous Mater.* **2004**, *69*, 149–155.
- (54) Nogami, M.; Tomozawa, M. Diffusion of water in high silica glasses at low temperature. *Phys. Chem. Glasses* **1984**, *25*, 82–85.
- (55) Nogami, M. Proton conduction in nanopore-controlled silica glasses. *J. Sol-Gel Sci. Technol.* **2004**, *31*, 359–364.
- (56) Nogami, M.; Nagao, R.; Wong, C. Proton conduction in porous silica glasses with high water content. *J. Phys. Chem. B* **1998**, *102*, 5772–5775.
- (57) Nogami, M.; Abe, Y. Evidence of water-cooperative proton conduction in silica glass. *Phys. Rev. B* **1997**, *55*, 12108–12112.